

Article

Numerical Study of Air Distribution and Thermal Environment in Attached Ventilation Mode in the Generator Layer of a Hydropower Station

Tong Ren *, Mengzhuo Li, Long He  and Panpan Sun

College of Mechanical and Electrical Engineering, Shaanxi University of Science and Technology, 6 Xuefu Middle Road, Weiyang University Park, Xi'an 710021, China; 230512141@sust.edu.cn (M.L.); helong@sust.edu.cn (L.H.); panpansunch@sust.edu.cn (P.S.)

* Correspondence: rentong@sust.edu.cn

Abstract: Because they are in enclosed underground buildings, the generator layers of hydropower stations have limited ventilation. In order to reduce the influence of a hot and humid environment on equipment and staff health and create a good thermal environment with good air quality for underground buildings, in this paper, vertical wall-attached ventilation was combined with the generator layer of a hydropower station to replace traditional ventilation. The influence of air supply velocity, air supply outlet position, and the opening mode of the generator layer on indoor velocity and temperature field distribution were analyzed via numerical simulation, and the evaluation indices of different cases were also compared. In the single-sided vertical wall-attached ventilation mode, when the velocity was increased from 4 m/s to 8 m/s, the maximum increment in the energy utilization coefficient was 41%, and the maximum reduction in the velocity non-uniformity coefficient was 9.5%. The results show that the single-sided mode can offer a higher ventilation efficiency than the double-sided mode, with a higher energy efficiency and a more uniform air distribution. Based on the mean temperature and velocity, and the key evaluation indices (head-foot temperature difference, percentage of dissatisfaction, non-uniformity coefficient, energy utilization coefficient, and air diffusion performance index), it is suggested that the single-sided air supply mode should be adopted for this kind of tall building, with an air supply velocity of $v = 6$ m/s and two open air supply outlets at each interval.

Keywords: generator layer; vertical wall attachment; numerical simulation; air distribution



Citation: Ren, T.; Li, M.; He, L.; Sun, P. Numerical Study of Air Distribution and Thermal Environment in Attached Ventilation Mode in the Generator Layer of a Hydropower Station. *Buildings* **2024**, *14*, 1030. <https://doi.org/10.3390/buildings14041030>

Academic Editor: Eusebio Z.E. Conceição

Received: 12 February 2024

Revised: 24 March 2024

Accepted: 2 April 2024

Published: 7 April 2024



Copyright: © 2024 by the authors. Licensee MDPI, Basel, Switzerland. This article is an open access article distributed under the terms and conditions of the Creative Commons Attribution (CC BY) license (<https://creativecommons.org/licenses/by/4.0/>).

1. Introduction

In the context of China's rapidly growing economy, building energy consumption in China accounts for about 46% of China's total energy consumption, and emissions reach 50% of the total emissions, ranking first in energy consumption and carbon emissions [1,2]. Among them, the energy consumption of ventilation and air conditioning systems inside building accounts for about 50–60%. Promoting energy saving ventilation and air conditioning systems and accelerating the development of green buildings are of great significance to realizing the goal of carbon peaking and carbon neutrality in the building field [3,4]. With the improvement of ventilation theory, the air distribution modes of mechanical ventilation mainly include mixed ventilation based on the dilution principle and displacement ventilation based on the displacement principle, these modes show different energy-saving advantages and ventilation effects under different applications [5–7]. With the in-depth study in the field of ventilation, some scholars focus on ventilation in underground buildings because of its complexity and necessity.

The ventilation of underground hydropower stations is facing a complex environment with high temperature and humidity, and the ventilation and air conditioning load of underground space changes dynamically. At the same time, with the long-term operation

of generator set, equipment aging and other factors may lead to heavy gas leakage [8–10]. However, with the existing ventilation mode, it is difficult to achieve the best environmental parameters for its large space, in the deep, buried, and complex structure of caverns [11]. Therefore, research on the most efficient and reasonable ventilation system is very important in hydropower stations to eliminate excess thermal and humid loads, ensuring a comfortable environment, the well-being of workers, and the stable operation of the equipment [12]. Taking the generator layer as an example, the factors affecting air distribution mainly include the following: the heat source, the number of air supply outlets, and the structural form [13]. At present, similar to the underground powerhouse of a hydropower station, several ventilation modes can be used depending on the space: (1) vault air supply, where the large section of the upper arch of a main building of the power station is used as a plenum, and a certain size and number of outlets are designed to supply air vertically; (2) displacement ventilation, where the existing air in the room is replaced by displacement ventilation, and cold air is directly sent into the room during work, so the ventilation efficiency is high; (3) stratified air conditioning air supply, where the basic principle is to control the generator layer by layer, which only provides air conditioning for the working area under the building, and does not take air conditioning for the upper area.

The above ventilation modes have been studied by scholars, showing different ventilation effects. Wang, Z.F. et al. analyzed the ventilation and air conditioning operation scheme of the main building of an underground power station with a uniform vault air supply when the generator set was in partial power generation operation conditions. The study put forward an hourly regulation strategy for the main powerhouse throughout the year, which improved the reference for the thermal environment and the operation regulation strategy of the hydropower station in cold areas [14]. Fu, X.Z. et al. conducted a model test to study the law of airflow for of the underground main building of Langyashan power station, analyzed the ventilation effect of the vault air supply in the main building under different air supply volume, velocity, temperature and outlet numbers, and put forward the air supply scheme [15]. Cheng, Z. et al. used Computational Fluid Dynamics (CFD) to study the air supply system of a stadium. The influences of different vent shapes on the air pressure ventilation characteristics were analyzed based on three aspects: the intake air volume, the depth of the airflow in the depth direction, and the wind speed in the main functional space; the optimal air supply mode was then proposed [16]. Wang, H.D. et al. adopted a method of combining experiments with CFD, to study the inter-regional heat transfer and load characteristics of a stratified air conditioning system for tall buildings under the action of exhaust air, focusing on the indoor vertical temperature trend, cooling load prediction, and the value of the inter-regional heat transfer coefficient [17]. Huang, C. et al. adopted a multi-node model to study the vertical temperature distributions under actual large space buildings with stratified air conditioning air supplies and verified them using field measurements [18]. Sun, Y.X. et al. put forward a displacement ventilation mode based on a square cylinder attachment for large space buildings, and further studied the ventilation effect of this mode and the thermal comfort in a building [19].

Stratified air conditioning, vault ventilation, and displacement ventilation have been widely applied in ventilation air conditioning systems for tall spaces, but they still have inevitable drawbacks [20]. When vault ventilation is used in a large space, because of the “full filling” of the airflow, the air supply jet first passes through the upper space of the building. Then, the mixed airflow is used to treat the load in the working area, which causes energy waste and low ventilation efficiency. The ventilation method of stratified air conditioning can effectively overcome these problems. However, the air outlet is usually located in the middle of a vertical wall; it is usually not conducive to the layout of the air supply pipeline and occupies a lot of building space. Displacement ventilation can achieve higher ventilation efficiency and better air quality. However, the air supply temperature difference and speed requirements limit displacement ventilation’s capacity to eliminate indoor load. In addition, the use of displacement ventilation often requires raising the height of the floor or occupying the effective space at the bottom of a building. To solve these

problems, this research group put forward a new air supply mode for a powerhouse in the tall space of an underground hydropower station combined with a vertical wall-attached air supply mode. Recently, jet ventilation has gained scholarly attention due to high momentum and favorable flow pattern [21–23], including impinging jet ventilation [24,25], attached plane jets, confluent jet ventilation and so on [26–28]. Compared with other air supply methods, the total cooling load borne by an attached air supply is smaller, which saves energy and does not affect the net height of a space.

Considering a building's structural features and the limitations of hybrid ventilation in tall spaces, the innovative approach of Square Column Attached Ventilation (SCAV) was introduced. This technique combines the benefits of hybrid and displacement ventilation, as depicted in Figure 1. SCAV is effective in achieving uniform air distribution and enhancing indoor thermal conditions [29,30]. This attached ventilation approach offers significant engineering advantages. It functions by directing air from a supply outlet into a working area, benefitting from the "support" provided by a vertical wall, which reduces mixing with surrounding air. After contacting the floor, the airflow changes direction horizontally, creating an attachment flow pattern on the floor. This results in a velocity distribution within the working area similar to that of displacement ventilation [31].

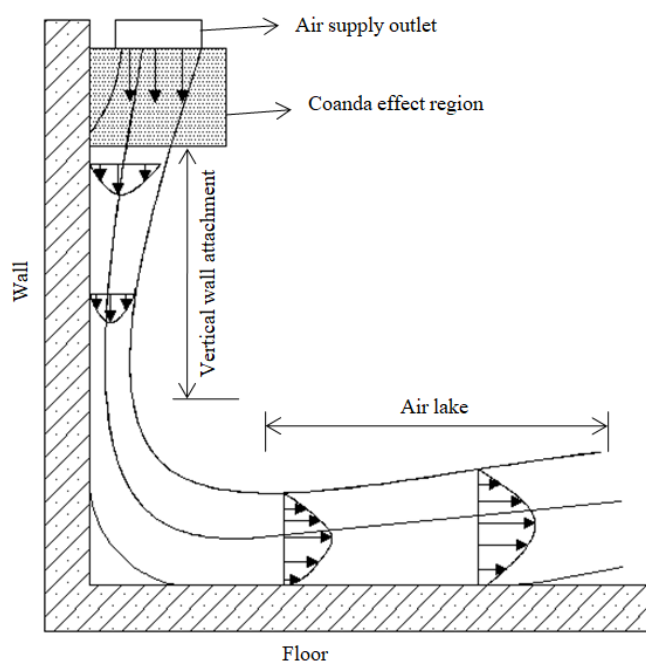


Figure 1. Schematic diagram of airflow structure under the vertical wall-based attached jet.

Research on the effects of wall impinging jet and displacement ventilation was also compared, and the flow characteristics of multiple confluent jets along vertical walls were studied. The results showed that the air distribution effect of the upper confluent jet mode was better than displacement ventilation [32,33]. Ye, M. et al. applied impinging jet ventilation systems in office buildings [34]. By comparing the airflow characteristics in the two heating modes of vertical wall impinging jet and mixed ventilation, Han, T. et al. found the vertical wall-attached jet ventilation can more effectively decrease heating energy consumption and improve the energy utilization coefficient. Meanwhile, this type of ventilation can make the ambient temperature field more uniform and effectively overcome the adverse effects of thermal buoyancy on indoor thermal comfort [35,36]. Vertical wall impinging jet is also applied to the ventilation design for high rooms, in which the multi-stream confluence wall impinging jet with parallel orifice nozzles impacted the corner flow ventilation mode with slit shaped outlets. The results showed that the behavior of the additional plane jet was different from the previous research in a relatively low room [37]. Li, A.G. et al. determined that air supply speed is the main parameter affecting

the airflow characteristics of this model. The temperature and velocity distribution are directly related to the room size and outlet position and are less affected by the location of the air vent. With reasonable parameter settings, the engineering application of a vertical wall-attached air supply mode in an existing building ventilation and air conditioning system can be realized [38,39]. They also studied and compared a vertical wall-attached jet with a deflector air supply and a layered air supply, and analyzed and compared the changes of air distribution characteristics of double-sided air supply modes with room height. It was found that both of these airflow forms can be very effectively delivered to the breathing zone, but the vertical wall-attached jet with a deflector can improve the thermal comfort for room staff [40].

Based on the above research results, the purpose of this paper was to study the thermal environment and air distribution within an underground hydropower station powerhouse with various vertical wall-attached air supply configurations. As shown in Figure 2, the study considered multiple air supply parameters, including air supply velocity, outlet positioning, and opening modes. The initial validation of the numerical model's reliability was performed using previously measured data [41]. This study assessed the results by analyzing velocity and temperature profiles to understand the impacts of supply velocity and patterns. Additionally, it examined the effects of head and foot temperatures, temperature and velocity uniformity coefficients, and energy utilization coefficients on environmental comfort. The research findings provide insights into optimizing cooling and air distribution within the underground hydropower station powerhouse.

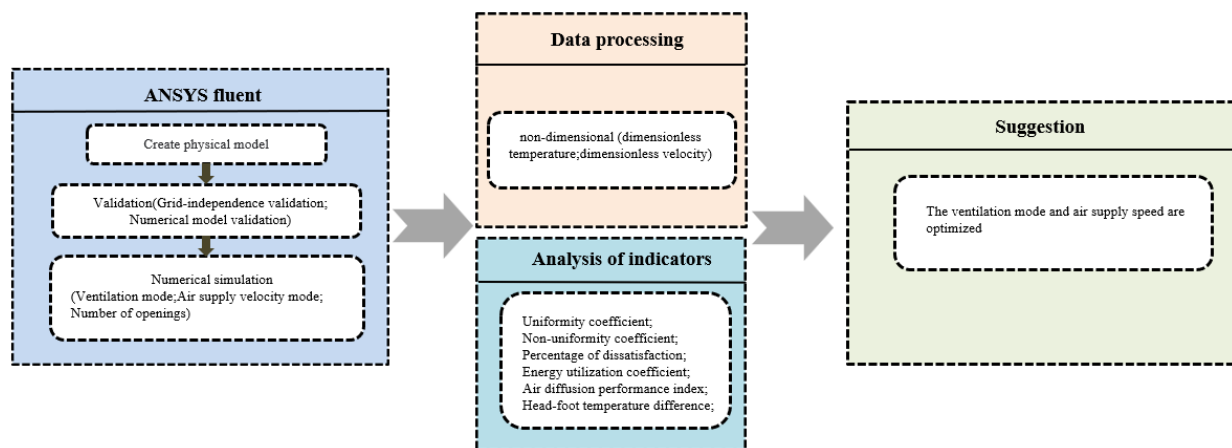


Figure 2. Flow chart of research methods for vertical wall-attached jet ventilation.

2. Research Methods

2.1. Geometric Settings and Assumptions

Taking the generator layer of an underground powerhouse as an example, the internal dimensions of the generator layer were $138 \times 24 \times 17 \text{ m}^3$ (L \times W \times H). The internal structure mainly includes the following sections: installation field; stairs and hanging holes (which are used for lifting and overhauling equipment); an air supply system for the generator hall; and heat generating equipment (the generator set heat, the power plate beside the machine, the transformer device and lighting).

In order to simplify the model, the curved arch roof was simplified into a flat plate, and the maintenance structure around it, the cover plate of the ground generator, the power panel, and the control panel beside the machine were simplified into a flat surface, as shown in Figure 3. At the same time, the air supply parameters in this paper are consistent with the design requirements of the actual project, the air supply temperature introduced through the traffic tunnel is 295 K. The wall temperature is assumed to remain constant during the process of air supply attached to the vertical wall. The hanging hole in the

generator layer is closed and the stairwell is normally open. Table 1 presents the design dimensions of the generator layer model.

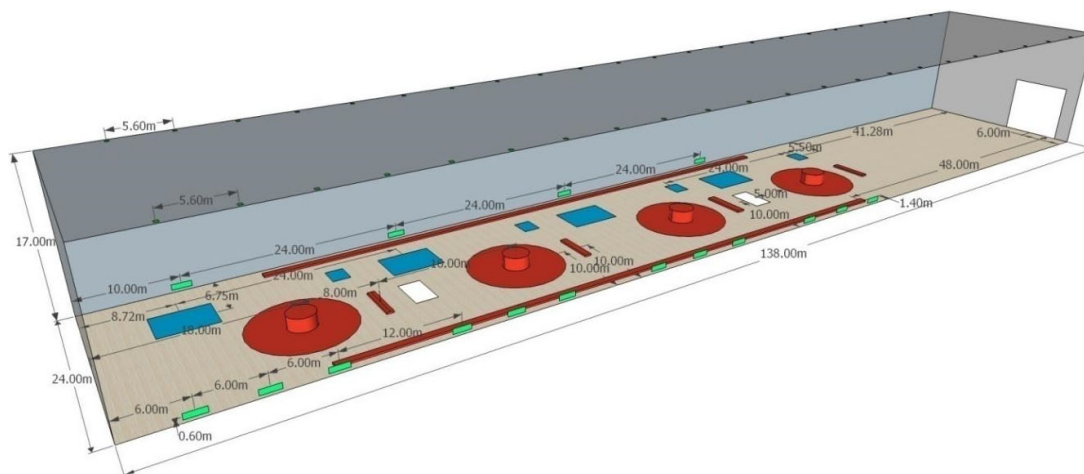


Figure 3. Three-dimensional geometry diagram of generator layer.

Table 1. The design parameters of the generator layer model.

Project	Size L × W × H (m ³)	Number	Velocity (m/s)	Temperature (K)
Generator layer size	138 × 24 × 17	-	-	-
Air supply vent	0.4 × 0.4	44	8	295
Upstream vents	2 × 0.6	4	-	-
Downstream vents	2 × 0.6	4	-	-
Downstream vents	2 × 0.6	4	-	-
Downstream vents	2 × 0.6	4	-	-
Hanging hole (large)	6 × 4.5	4	-	-
Hanging hole (small)	2 × 2.5	4	-	-
Stairs	2.5 × 4.5	2	-	-
Traffic hole	8 × 8	1	0.2	295
Wall	-	6	-	293

The heat in the generator layer was mainly from the generator set heat, the power plate beside the machine, the transformer device of the control panel beside the machine, the heat brought into the air through the traffic tunnel, the illumination, and so on [39]. For the convenience of this study, the body heat source of the generator layer was simplified as a corresponding surface heat source and the intensity of each body heat source was simplified into a corresponding surface heat flux. The heat source in the model was simplified into a strip or circle shape. The simplified heat source sizes and heat flux parameters are shown in Table 2.

To efficiently manage the air quality in the generator layer, it was imperative to implement suitable air supply configurations. According to the structural characteristics of the generator layer, the vertical wall attachment should rely on the length direction for air supply. Based on the existing vent design, the air outlet layout strategy for the vertical wall-attached jet ventilation mode could be formulated as follows:

- (1) Scheme 1: Double-sided air supply. The air supply vents were positioned on the ceiling of the generator layer close to the wall surface, and 2 rows were evenly arranged, with 22 air supply outlets each row. See Figure 4a.

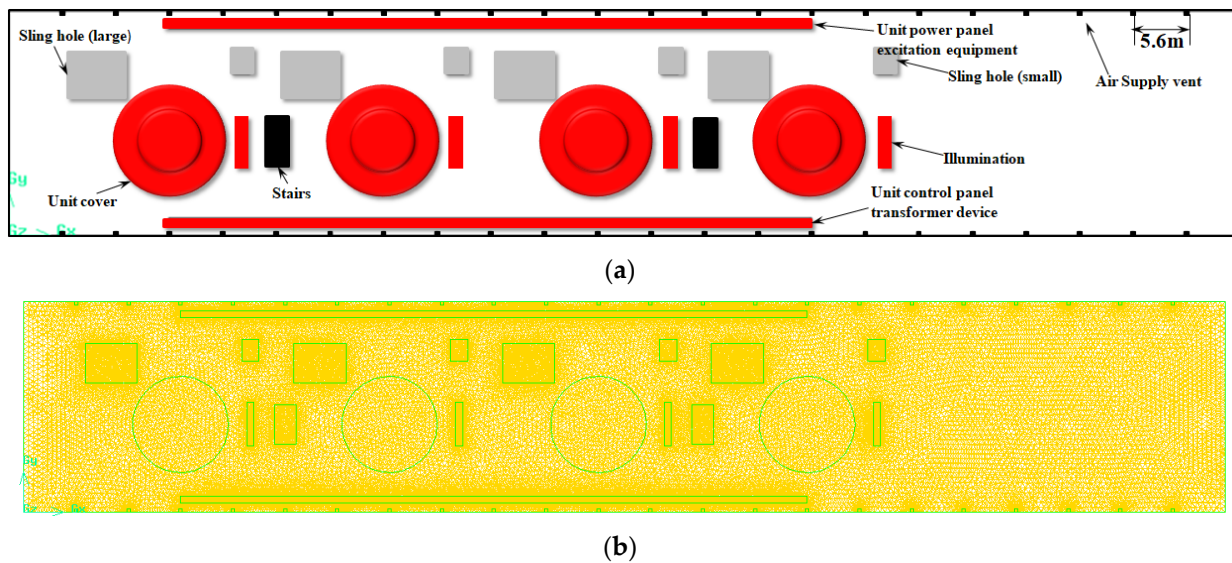


Figure 4. (a) Arrangement of double-sided vents; (b) meshing of double-sided vents (Model 1).

- (2) Scheme 2: One-sided air supply. The air supply vents were arranged on the ceiling of the left side of the generator layer close to the wall surface, and a row was evenly arranged, with 44 air supply outlets. See Figure 5a.

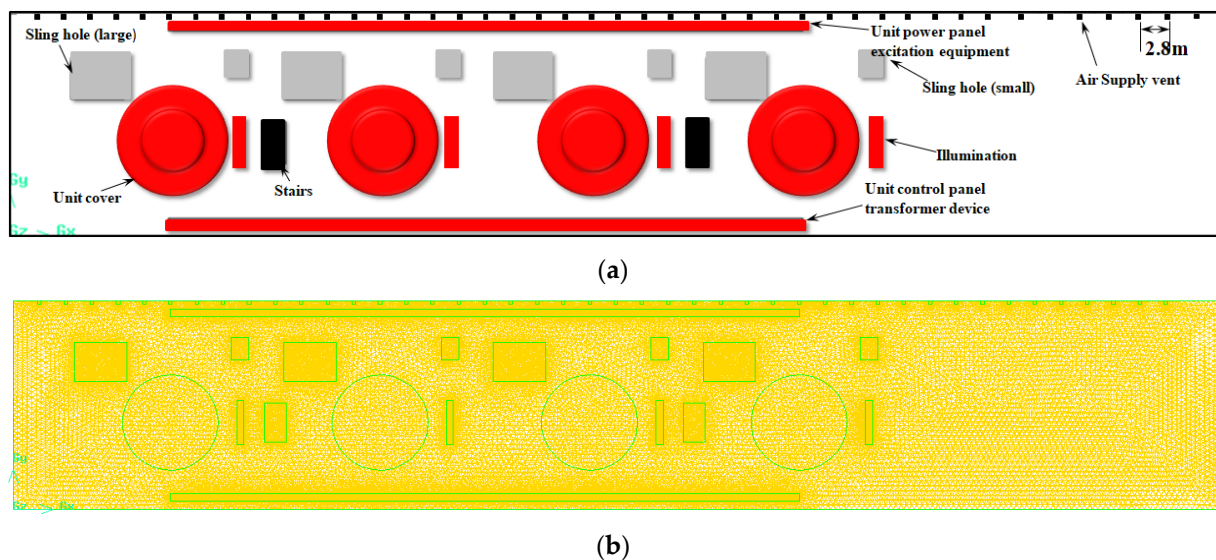


Figure 5. (a) Arrangement of single-sided vents; (b) meshing of single-sided vents (Model 2).

Figures 4b and 5b are schematic diagrams of the grid divisions of the numerical calculation area of the generator layer in three-dimensional vertical wall-attached air supply model. Grid encryption was carried out for the air supply outlet, air return outlet area, vertical wall-attached area, transverse ground air lake area, and near-wall area, because these areas had high change rates caused by momentum changes and heat transfer.

Table 2. The parameters of the generator layer heat source model.

Project.	Heat Release (kW)	Size L × W (m ²)	Heat Flux Density (W/m ²)	Number	Simplified Shape
Unit cover Air leakage of generator set	56.0 35.2	r = 5.5	240	4	Circular heat source
Unit power panel excitation equipment	54.4	72 × 0.8	944	1	Upstream heat source
Unit control panel transformer device	54.3	72 × 0.8	944	1	Downstream heat source
Illumination	15.1	0.8 × 5	944	4	Midstream heat source

2.2. Setting Working Conditions

In this paper, the effect of a vertical wall-attached air supply on ambient air quality was studied. It was important to maintain the same supply air temperature, traffic hole inlet air velocity, and temperature. Therefore, the effect of the changes in the air supply velocity, opening mode, and number of air supply outlet on the air distribution of a vertical wall-attached was analyzed. See Table 3 for the specific working conditions.

Table 3. Simulated working conditions table.

Case	Model	Air Supply Velocity (m/s)	Supply Air Temperature (K)	Traffic Hole Inlet Air Velocity (m/s)	Traffic Hole Inlet Air Temperature (K)	Wall Temperature (K)	Opening Mode of Air Supply Outlet
A	1	8	295	0.2	295	293	Open all
B	1	6	295	0.2	295	293	Open all
C	1	4	295	0.2	295	293	Open all
D	1	8	295	0.2	295	293	Open two at each interval
E	1	8	295	0.2	295	293	Open one at each interval
A1	2	8	295	0.2	295	293	Open all
B1	2	6	295	0.2	295	293	Open all
C1	2	4	295	0.2	295	293	Open all
D1	2	8	295	0.2	295	293	Open two at each interval
E1	2	8	295	0.2	295	293	Open one at each interval
F	2	8	295	0.2	295	293	Open one at intervals of two

2.3. Selection of Monitoring Points

In order to display the working environment of the generator layer more effectively under in different cases, two monitoring lines were selected at a height of $z = 1.7$ m. Twenty monitoring points were uniformly arranged on line 1 and labeled as measuring points 1–20. Another twenty detection points were evenly arranged on line 2, and their labels are measuring points 21–40. Figure 6 is a schematic diagram of the detection points on the generator layer.

Fluent 19.2 was employed to create a transient three-dimensional model to simulate the airflow distribution. The finite volume method was employed to discretize the governing equations. The discrete equations obtained via the finite volume method had good integral conservation, and the integral conservation of characteristic variables is required to satisfy any set of control volumes. All surfaces of the wall were provided as non-roughness anti-skid walls and have standard wall function for treating near-wall areas. SIMPLEC algorithm was used to solve the flow field. This algorithm considers the neglected part of the SIMPLE algorithm, which affects the velocity of surrounding nodes, and has better convergence. The discretization of convection terms, encompassing momentum, energy, and

turbulence equations employed a second-order upwind numerical scheme. Convergence was determined based on continuity, with the condition that the absolute residuals of the momentum and turbulence equations should not exceed 10^{-3} , while the residuals of the energy equations should remain below 10^{-6} .

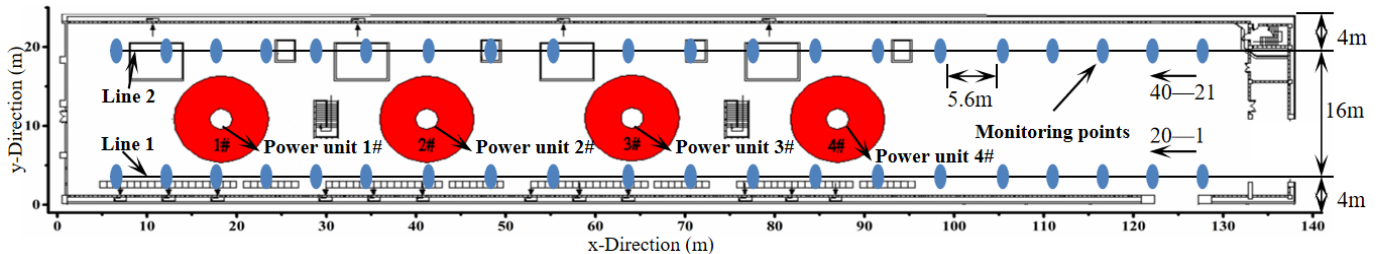


Figure 6. Monitoring points in the generator layer.

2.4. Boundary Conditions

Boundary conditions and initial conditions are necessary for solving CFD problems, which represent the variation laws of variables or their first derivative on the boundary of a solution domain with a place and time. Only when reasonable boundary conditions and initial conditions are given can the solution of a flow field be calculated. In the vertical wall-attached jet ventilation mode, airflow was considered incompressible, and the boundary conditions for the generator layer of the hydropower station were established as follows:

- (1) Inlet boundary condition: velocity inlet boundary condition, the simulated air supply speeds are, respectively, 8 m/s, 6 m/s, and 4 m/s.
- (2) Boundary condition of the return air outlet: pressure outlet.
- (3) Wall boundary conditions: static walls were adopted without sliding for the generator layer walls.
- (4) Boundary conditions of the heat source: The heat source of the unit cover was regarded as constant heat flux, and the heat flux density was 240 W/m^2 . The excitation equipment of the power panel and the transformer device of the control panel were regarded as constant heat flux, and the heat flux was 944 W/m^2 . The heat flux density data were converted based on measured equivalence [39].

2.5. Grid-Independence Validation

The verification of grid number independence was mainly to check the simulation results of the calculation model using different grid numbers, and to determine the appropriate number of grid division system. In this section, A fine grid, a medium grid, and a coarse grid were used for comparison, with corresponding grid numbers of 2,067,863, 1,379,585, and 788,217, respectively. To assess the grid independence, temperatures were extracted evenly from various height planes ranging from 0 to 17 m, (see Figure 7). The results indicate that when the grid number reaches 2.07 million, there was only a slight temperature fluctuation along the height direction within the model. The mean error between the grid numbers of 1,379,585 and 2,067,863 was 0.067%, with a maximum error of 0.081%. The latter error falls within an acceptable range. Therefore, the model with a grid number of 1,379,585 was chosen for the simulation to optimize computational time and efficiency.

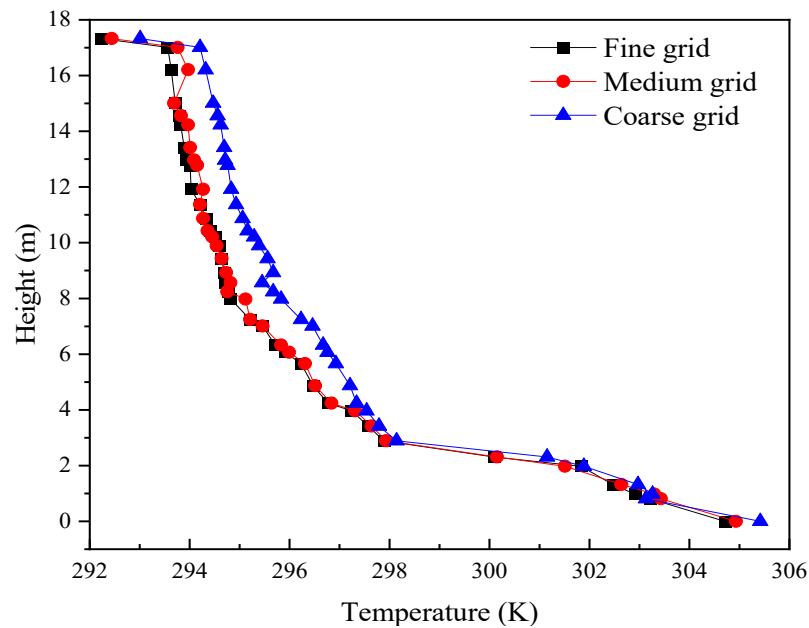


Figure 7. Model mesh independence verification.

2.6. Numerical Model Validation

Because of numerical simulation's attributes of precision, speed, and cost-effectiveness, it is widely used to analyze and optimize the ambient airflow distribution [42–44]. The $k-\epsilon$ two-equation model is the most widely used turbulence model and has many deformation forms. In the model, k is the turbulent kinetic energy term, ϵ is the dissipation rate term of the turbulent kinetic energy, and the combination of the two can obtain the turbulent eddy viscosity, which makes the turbulent time-mean equations close, and then solve the numerical solution. Yin, H.G. [30] used four different turbulence models, namely the Standard $k-\epsilon$ model, RNG $k-\epsilon$ model, SST $k-\epsilon$ model, and RSM-IP model to simulate and analyze the vertical wall-attached jet, and the results showed that in terms of predicting indoor airflow organization, the SST $k-\epsilon$ model is superior to the RNG $k-\epsilon$ model, and both of them can effectively predict the flow field distribution of a vertical wall-attached jet. However, for the square cylindrical attached jet mode, the numerical calculation results using the Realizable $k-\epsilon$ model agree well with the experimental data [32]. Li, Y.J. chose the RNG $k-\epsilon$ model and Realizable $k-\epsilon$ model for comparative analysis when studying a non-isothermal vertical wall-attached jet, and finally adopted the Realizable $k-\epsilon$ turbulence model for research [45]. Comparatively, the shaft temperature at the air supply outlet is extracted and subsequently compared between simulation and the field test results. The field test temperatures were recorded using a temperature and humidity module, ranging from 0 to 8 meters, with measuring points spaced 1 meter apart [41]. The placement of the testing apparatus and test points is depicted in Figure 8.

In Figure 9, a comparison is presented between the measured and simulated shaft temperatures of the air supply outlet, spanning from 0 to 8 m. It can be seen that the numerical model was consistent with the test results below a height of 5 m, there were some discrepancies between the tested and simulated results at heights over 5 m. This was due to the fact that the attached wall was set to an equal wall temperature in the simulation, and the wall temperature value was the measured temperature of the lower wall area for the test condition constraints. However, the actual wall surface temperature varied from top to bottom, and the upper wall temperature was low. Therefore, the temperature values in the test were lower at heights over 5 m. After the calculation, the maximum deviations between the test results and the Standard $k-\epsilon$, RNG $k-\epsilon$, and Realizable $k-\epsilon$ is 1.07 K, 0.75 K, and 0.90 K, respectively. Notably, the Realizable $k-\epsilon$ model demonstrated a temperature match to the test results with mean deviation of 1.76%, which met the accuracy requirements. Consequently, the Realizable $k-\epsilon$ model was chosen for further calculations.

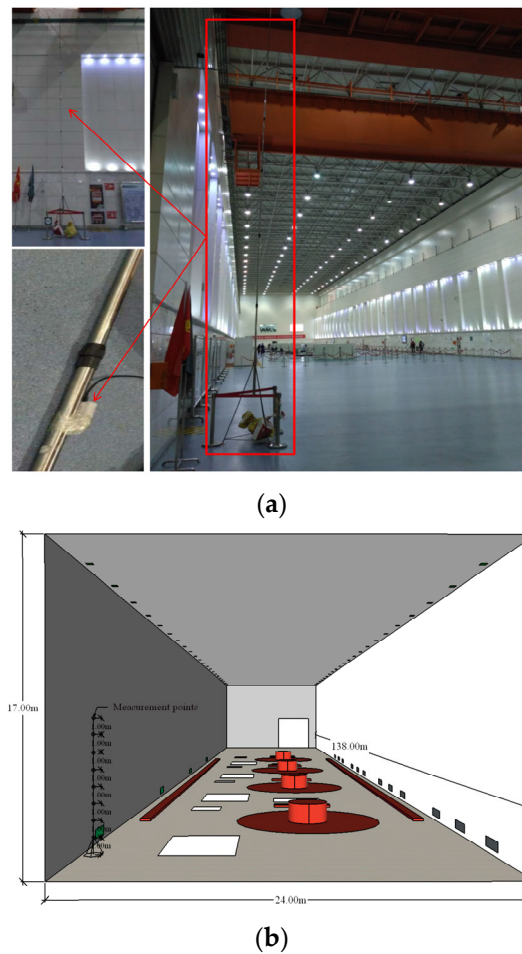


Figure 8. (a) The position of the test device; (b) arrangement of measuring points.

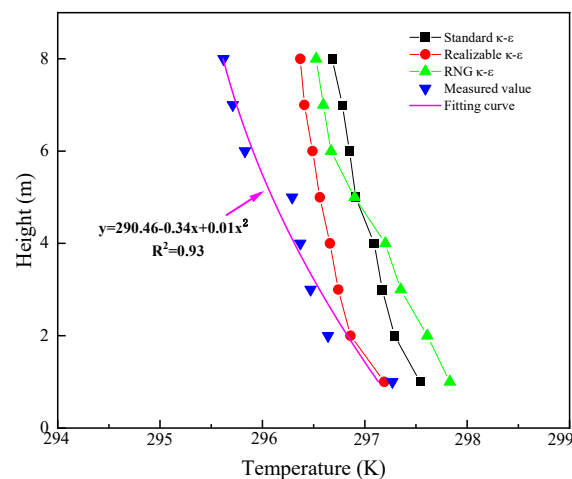


Figure 9. Measured and simulated variations in the shaft temperature of air supply outlet.

As shown in Figure 10, the numerical results show that the jet velocity decreases gradually along the wall height under the vertical wall-attached air supply mode. It shows a similar velocity attenuation law under different air supply velocities. Airflow jet velocity attenuation can be calculated by exponential expression (1), which is basically consistent with the results given by the literature [46]. In this reference, the air supply velocity is

8 m/s, the air supply temperature is 308 K. The maximum relative error between them is 23%, this may be caused by different supply air temperatures.

$$U = 4.17 - 3.97 / (1 + \exp(h^* - 1.21/0.16)) R^2 = 0.98 \quad (1)$$

where h^* is a dimensionless height, $h^* = h/H$, h is height of measuring point (m), H is the height of the generator floor (m), U is a dimensionless velocity.

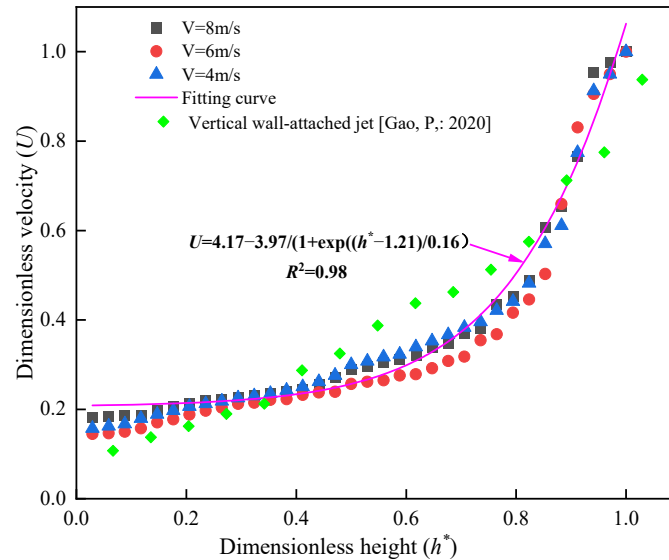


Figure 10. Jet velocity attenuation of the air supply outlet under different velocities [46].

3. Processing Method of Testing Data and Evaluation Indexes

In this paper, the velocity and temperature are treated as dimensionless. At the same time, head-foot temperature difference, percentage of dissatisfaction, uniformity coefficient, energy utilization coefficient, and air diffusion performance index are mainly used to appraise and analyze the airflow organization of the factory building.

3.1. Dimensionless Temperature

In this study, in order to evenly compare the temperature changes under different working conditions, dimensionless temperature is adopted, which is determined by the following formula [47]:

$$\theta = \frac{t_i - t_0}{t_e - t_0} \quad (2)$$

where θ is the dimensionless temperature, t_i is the temperature at measuring point, K. t_0 is the supply air temperature, K. t_e is the exhaust air temperature, K.

3.2. Dimensionless Velocity

Dimensionless velocity is convenient to compare the change of airflow velocity under different velocity conditions. The formula is as follows:

$$U = \frac{v_i}{V} \quad (3)$$

U is dimensionless velocity. v_i is the velocity of measuring point, m/s. V is the air supply velocity in the generator floor, m/s.

3.3. Head-Foot Temperature Difference

The head-foot temperature difference in a working area serves as an important indicator for evaluating human body thermal comfort. To determine the thermal comfort needs

of individuals in workspaces and ensure indoor air quality, design standards dictate the following requirement.

The head-foot temperature difference with a standing posture [35]:

$$|\Delta t_{1.7-0.1}| \leq 3K \quad (4)$$

The above formula Δt is the standing head and foot temperature difference, K.

3.4. Percentage of Dissatisfaction (PD)

When the air supply airflow differs from the air temperature in space, it results in a vertical temperature gradient in the height direction. A high vertical temperature difference between the head and the ankles can lead to local discomfort, which is expressed as percentage dissatisfied (PD) [48]. PD can be calculated by the following formula:

$$PD = \frac{100}{1 + \exp(5.76 - 0.856 \times \Delta t)} \quad (5)$$

3.5. Non-Uniformity Coefficient

The vertical wall-attached jet model's mechanism relies on the formation of an air lake-like pattern for velocity and temperature distribution within a workspace. Achieving this air lake formation necessitates a uniform velocity and temperature field. The uniformity of airflow is primarily assessed using velocity and temperature non-uniformity coefficients, as follows [47]:

$$k_v = \frac{\frac{1}{n} \sum_{i=1}^n (v_i - \bar{v})^2}{\bar{v}} \quad (6)$$

$$k_t = \frac{\frac{1}{n} \sum_{i=1}^n (t_i - \bar{t})^2}{\bar{t}} \quad (7)$$

In the above formula, k_v is the uniformity coefficient of the velocity, k_t is the uniformity coefficient of the temperature, n is the number of measuring points, v_i and t_i are the velocity and temperature at each measuring point, \bar{v} is the mean velocity, m/s. \bar{t} is the temperature, K.

3.6. Energy Utilization Coefficient

The selection of the indoor air energy utilization coefficient distribution scheme directly affects the performance of the ventilation and air conditioning system. In order to evaluate the energy utilization of different working conditions, the efficiency of the energy utilization of air distribution was investigated [46]:

$$\eta = \frac{t_e - t_0}{t_n - t_0} \quad (8)$$

In the formula, t_e is the exhaust air temperature, K. t_n is the average air temperature in the working area, K. t_0 is the supply air temperature, K. If $\eta = 1$, it indicates that the supply air absorbs the residual heat to reach the indoor temperature, and then discharges together. If $\eta > 1$, it indicates the supply air absorbs waste heat, and can control the temperature of the personnel activity area. Therefore, the economy is good. If $\eta < 1$, it indicates that the input energy has not been fully utilized, generally, due to short circuit and failed to play the role of air heat; therefore, the economy is poor.

3.7. Air Diffusion Performance Index (ADPI)

ADPI takes into account the effects of air temperature and wind speed on the human body, which is defined as the percentage of the occupied zone falling into the accept-

able velocity and temperature region determined by measuring the local Effective Draft Temperature (EDT) [30].

$$EDT = (t_i - t_n) - 7.66(v_i - 0.15) \quad (9)$$

$$ADPI = \frac{\text{Number of measuring points}(-1.7K \leq EDT \leq +1.0K)}{\text{The total number of measuring points}} \times 100\% \quad (10)$$

where t_i is air temperature at the measuring point in the workspace, K. t_n is the indoor air temperature, K. v_i is air velocity at the measuring point in the workspace, (m/s).

4. Results and Discussion

4.1. The Effect of Air Supply Velocity

Figure 11 illustrates the velocity distribution at $z = 1.7$ m in the generator layer under the vertical wall impinging jet mode with a double-sided air supply. The data directly reflects the airflow speed in the $z = 1.7$ m section. As the air supply speed increases, the airflow speed in the working area also rose. This velocity pattern remained consistent when the supply air temperature and outlet position were unchanged, despite variations in the air supply velocity. When the supply air velocity reached 8 m/s, the airflow speed in the work area exceeded 0.2 m/s, with a mean airflow velocity of 0.55 m/s. However, some areas experienced airflow velocities exceeding 0.8 m/s, which might lead to discomfort. When $v = 6$ m/s, the velocity distribution was more uniform at $z = 1.7$ m, and the mean velocity across all regions was 0.37 m/s. With an air supply velocity of 4 m/s, most areas in the $z = 1.7$ m section exhibit airflow velocities that did not exceed 0.2 m/s, which did not meet the relevant code requirements. Comparing these three air supply conditions, the case of $v = 6$ m/s provided improved comfort for personnel.

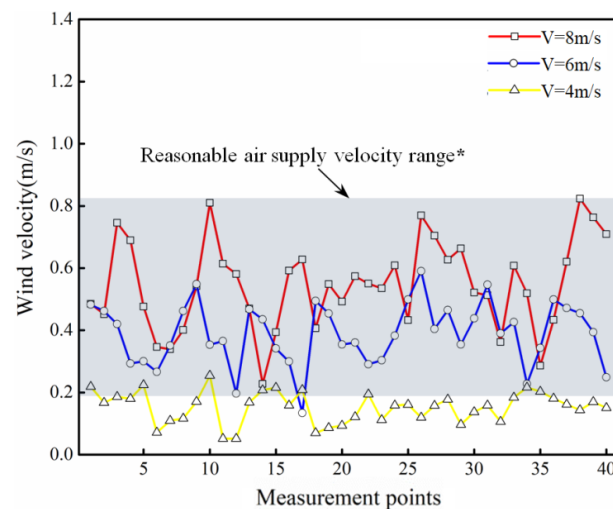


Figure 11. Velocity distribution of the double-sided mode under different air supply velocities. (* The reasonable air supply velocity range is between 0.2 m/s and 0.8 m/s, the same as below).

In Figure 12, the velocity distribution in $z = 1.7$ m section with a one-sided air supply is presented for different air supply velocities. When the supply air velocity reached 8 m/s, the airflow speed exceeded 0.8 m/s in most areas, with a mean velocity of 0.93 m/s, this would cause discomfort to personnel and would not comply with the relevant specifications. When $v = 6$ m/s, the air velocity surpassed 0.2 m/s, with a mean velocity of 0.66 m/s, but a few areas still had velocities exceeding 0.8 m/s. With an air supply velocity 4 m/s, the airflow velocity meets the relevant code requirements, with a mean velocity of 0.45 m/s. Additionally, for the one-sided air supply configuration, the airflow speed in the working area is greater than that in a two-sided air supply setup. This was due to the smaller air

supply vent spacing in the single-sided air supply mode, The supply air supported each other, resulting in less air diffusion, so the air could be effectively sent into the work area.

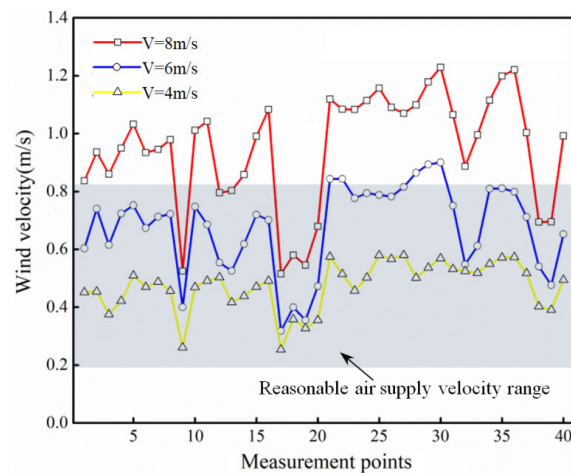


Figure 12. Velocity distribution of the single-sided mode under different air supply velocities.

Figure 13 is the velocity nephogram at $x = 60$ m of generator layer cross section under different airflow velocities, and different air supply speeds lead to different effects. The high momentum jet discharged from the vent deviates from the nearby wall and then adheres to the surface. The inclination of the jet was promoted to tilt towards the wall, and sufficient adhesion is realized in the vertical wall area. For the case of double-sided air supply (Case A, B, C), when $v = 8$ m/s, the mean airflow velocity at the cross section is 0.47 m/s. When $v = 6$ m/s, the mean velocity is 0.33 m/s. When $v = 4$ m/s, the mean velocity at the cross section is 0.21 m/s. However, in the case of one-sided air supply (Case A1, B1, C1), when $v = 8$ m/s, the mean velocity at the cross section is 0.72 m/s. When $v = 6$ m/s, the mean velocity is 0.54 m/s. When $v = 4$ m/s, the mean airflow velocity at the cross section is 0.34 m/s. As air supply velocity increases, an “air lake” effect, similar to displacement ventilation in the working area, becomes more pronounced. Additionally, the presence of vortices within the room significantly enhances indoor air circulation, with the circulation effect becoming more evident as airflow velocity increases. Notably, in the case of one-sided air supply, the airflow velocity is higher than that of two-sided air supply mode.

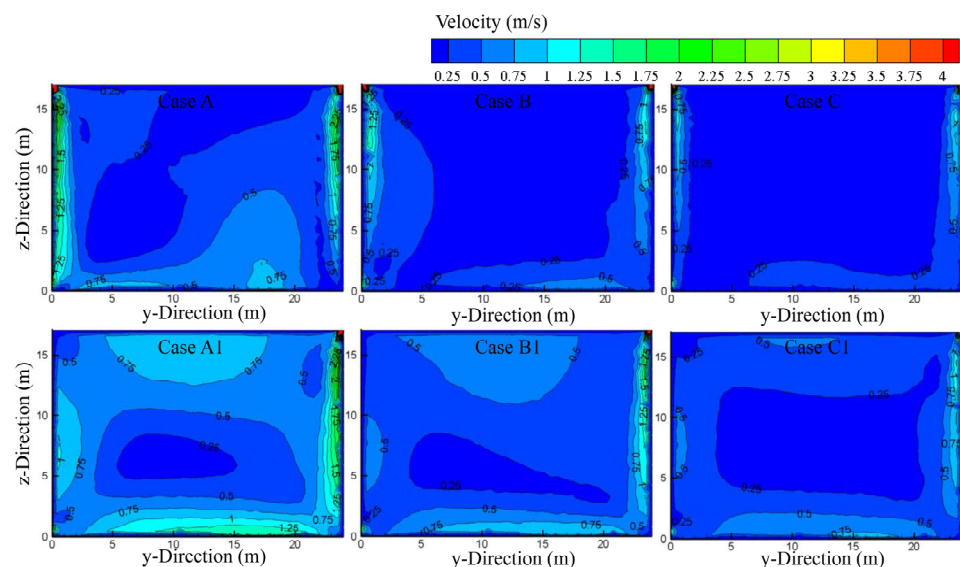


Figure 13. Velocity nephogram under different air supply velocities ($x = 60$ m).

Figure 14 shows the dimensionless temperature distribution in the working area under different air supply velocities in the double-sided air supply mode. It could be seen that in the installation field area of the hydropower station (measuring points 1–5 and 20–25), the dimensionless temperature was low. With the increase in air supply velocity, the temperature in this region did not change obviously, because there was no unit heat source in the area, and cold air could be directly delivered. And, the dimensionless temperature in the generator set area was relatively high due to the existence of heat sources. With the increase in the air supply velocity, the cold air can fully exchange the heat with the ambient air, showing that the temperature of the working area was gradually reduced. It could also be seen that when the air supply speed was reduced from 8 m/s to 6 m/s, the dimensionless temperature in the working area did not change significantly, while when the air supply speed was reduced to 4 m/s, the temperature increases greatly.

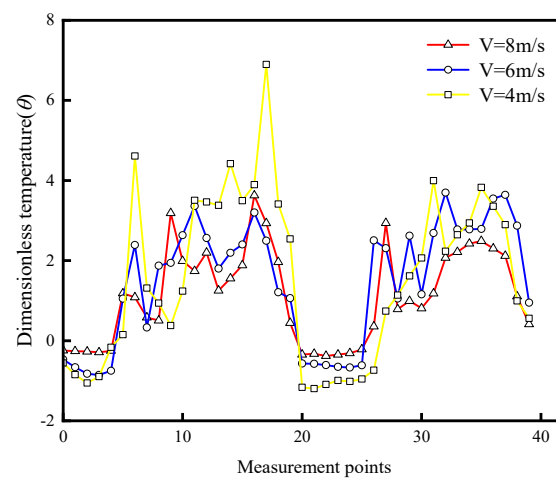


Figure 14. Temperature distribution of the double-sided mode under different air supply velocities.

Figure 15 shows the dimensionless temperature distribution in the working area under different air supply velocities in single-sided air supply mode. It could be seen that in the installation area (measuring points 1–5 and 20–25), the dimensionless temperature was still low, which was consistent with the results of double-sided air supply. The dimensionless temperature in the generator set area was relatively high and did not change significantly with the decrease in the air supply speed from 8 m/s to 4 m/s. This showed that under the single-sided air supply mode, the airflow with different air supply speeds reached the working area and achieved full heat exchange.

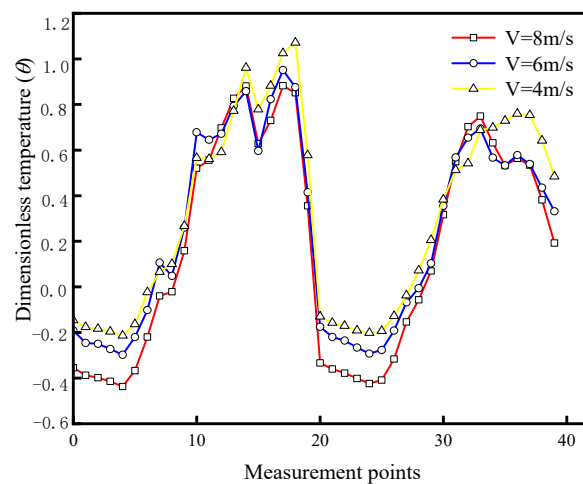


Figure 15. Temperature distribution of the single-sided mode under different air supply velocities.

The temperature at $z = 1.7$ m followed a consistent pattern when air supply temperature and outlet positions were identical, even with varying air supply velocities. Measuring points 1 and 21 showed lower temperatures, being distant from the heat source. As one moved closer to the heat source from measuring points 1 to 20 and from measuring points 21 to 40, the temperature gradually increased. At the same velocity, one-sided air supply in the $z = 1.7$ m section exhibited higher temperature uniformity compared to the two-sided air supply. Analyzing the impact of airflow velocity changes on the working zone temperature, it could be seen that with the increase in the air supply speed, the uniformity of the temperature in the working area was improved.

Figure 16 displays the temperature field of the generator layer cross-section at various air supply velocities. In the factory building area, the temperature distribution exhibits a similar trend, but different airflow velocities result in noticeable stratification. Higher airflow velocities produce a more pronounced cooling effect on the working area. Specifically, air supply velocities ranging from 8 to 4 m/s show that single-sided air supply (Case A, B, C) yields a stronger overall cooling effect than double-sided air supply (Case A1, B1, C1). When the air supply speed is consistent, the mean temperature difference between the two models is approximately 1 K. Just as the above analysis of the velocity field, the working area speed under the single-sided mode is larger, resulting in a more effective flow of cold air into the working area, making the working area carry out sufficient heat exchange. Therefore, it can be seen the working area temperature is lower under the single-sided mode.

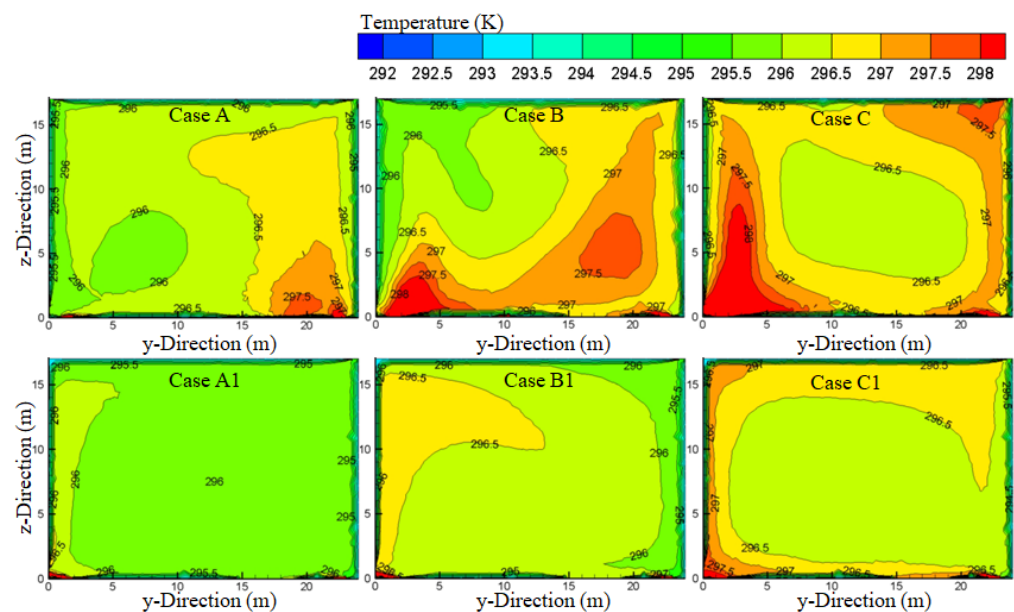


Figure 16. Temperature nephogram under different air supply velocities ($x = 60$ m).

Table 4 presents the assessment parameters for the two vertical wall-attached air supply modes at different velocities. The head-foot temperature difference remained well below 3 K and the PD values were all less than 3% (in Category A [48]) for both modes, fully meeting the design standards. The single-sided mode (Cases A1, B1, and C1) exhibited a higher η and ADPI compared to the double-sided mode (Cases A, B, and C). For the single-sided mode, with the increase in the supply velocity, the energy utilization coefficient first increases and then decreases. Increasing the velocity from 4 m/s to 8 m/s led to a maximum ADPI value 70% (A1), a maximum 41% increase in η (Case B1), a maximum 9.5% reduction in k_v (Case B1), and a maximum 34% reduction in k_t (Case B1). The single-sided mode demonstrates lower velocity and temperature non-uniformity compared to the double-sided mode, indicating superior uniformity in the entire airflow field.

Table 4. Evaluation indicators under different velocities.

Case	Head-Foot Temperature Difference (Δt)	Percentage of Dissatisfaction (%)	Energy Utilization Coefficient (η)	Velocity Non-Uniformity Coefficient (Kv)	Temperature Non-Uniformity Coefficient (Kt)	Air Diffusion Performance Index (ADPI) (%)	Percentage of Dissatisfaction (%)	Air Diffusion Performance Index (ADPI) (%)
A	0.55	0.5020	1.02	0.2583	0.0035	62.5	0.5020	62.5
B	0.93	0.6937	1.01	0.2740	0.0040	50	0.6937	50
C	1.16	0.6933	1.07	0.4529	0.0086	30	0.6933	30
A1	0.57	0.5106	3.38	0.2090	0.0024	70	0.5106	70
B1	0.79	0.6158	4.77	0.2275	0.0029	57.5	0.6158	57.5
C1	1.23	0.8949	4.11	0.2492	0.0039	35	0.8949	35

4.2. Opening Mode of Air Supply Outlet

Figure 17 shows the dimensionless speed distribution of the working area under different opening modes in the double-sided air supply. It could be seen that when all air outlets are opened (Case A), the dimensionless velocity of the workspace reaches its maximum. As the number of openings decreases, the dimensionless speed of the working area decreases gradually. Because the total supply air volume in the work area was also reduced, it could also be seen that the working area speed of all working conditions is basically within the reasonable air supply velocity range. It could also be seen that the three air supply modes can effectively send cold air to the working area.

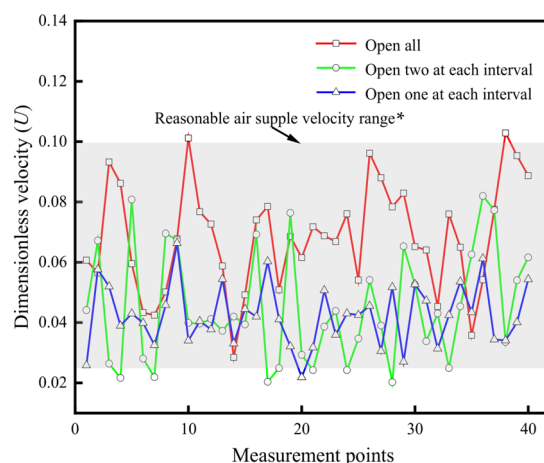


Figure 17. Velocity distribution of the double-sided air supply under different opening modes. (* The reasonable air supply velocity range between dimensionless velocity 0.25 and 0.10, the same as below).

Figure 18 shows the dimensionless speed distribution of the working area under different opening modes in the single-sided air supply. It can be seen that the dimensionless velocity of the working area decreases gradually with the decrease in the number of openings. When all air outlets are opened (Case A1), the dimensionless velocity of the workspace reaches its maximum and exceeds the range of reasonable supply air velocity, showing the difference from the double-sided supply mode. Similarly, when opening one at an interval of two (Case F), the air supply speed in some working areas was lower than the required speed range. It could also be seen that in the Cases D1 and E1, the working area speed was basically within a reasonable velocity range.

Figures 19 and 20 show the dimensionless temperature distribution under different opening modes. It could be seen that dimensionless temperature in the working area gradually decreased with the decrease in the number of openings in the double-sided air supply mode. However, for the single-sided air supply mode, the change of the opening numbers had little effect on the dimensionless temperature of the working area. Moreover, the dimensionless temperature of single-sided air supply mode was significantly lower than that of double-sided air supply mode. Therefore, it can be concluded that the single-sided

air supply mode could effectively reduce the ambient temperature of the working area and achieve a better ventilation effect.

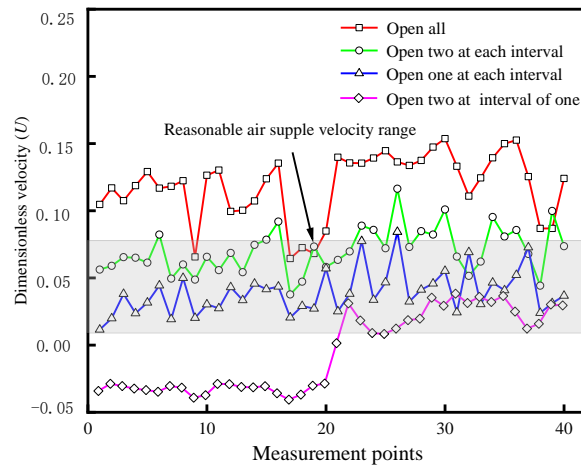


Figure 18. Velocity distribution of the single-sided air supply under different opening modes.

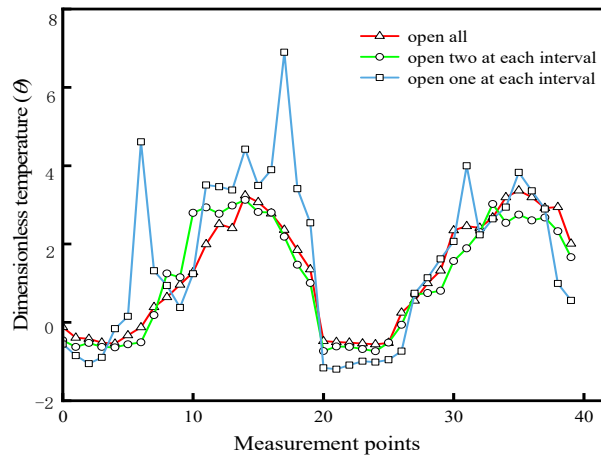


Figure 19. The temperature distribution of the double-sided air supply under different opening modes.

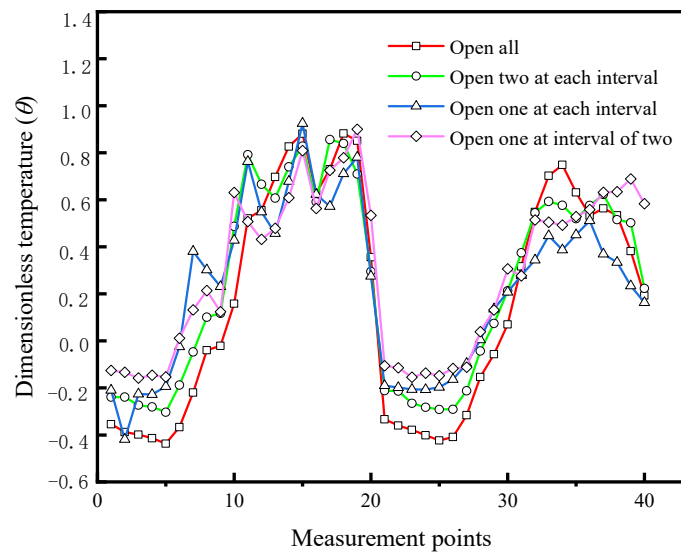


Figure 20. Temperature distribution of the single-sided air supply under different opening modes.

Based on the analysis, the influence of different opening modes on the speed and temperature of the working area was relatively obvious. However, when the number of openings was reduced to a certain number, the temperature and speed of the working area exceeded the design requirements, and this result is especially obvious when the position of the air supply outlet changes.

4.3. The Positioning of Air Supply Outlet

Figure 21 compares the working area temperature and velocity at $z = 1.7$ m under different positions of air supply outlets. It could be seen that the air can be more effectively fed into the working area under the single-sided air supply mode (Case A1), and the velocity distribution was higher than double-sided air supply mode, especially in the unit heat source position. Under the same air supply volume, the outlet spacing of single-sided air supply mode was closer, resulting in a smaller controlled area for each outlet and thus a better ventilation effect. Figure 21b shows that the working area temperature under the single-sided air supply mode was lower than that of double-sided air supply mode, and the temperature distribution was more uniform. On the contrary, the temperature of double-sided air supply mode was higher in the local area. Because the air supply airflow in this area had not been effectively delivered, the heat exchange was insufficient.

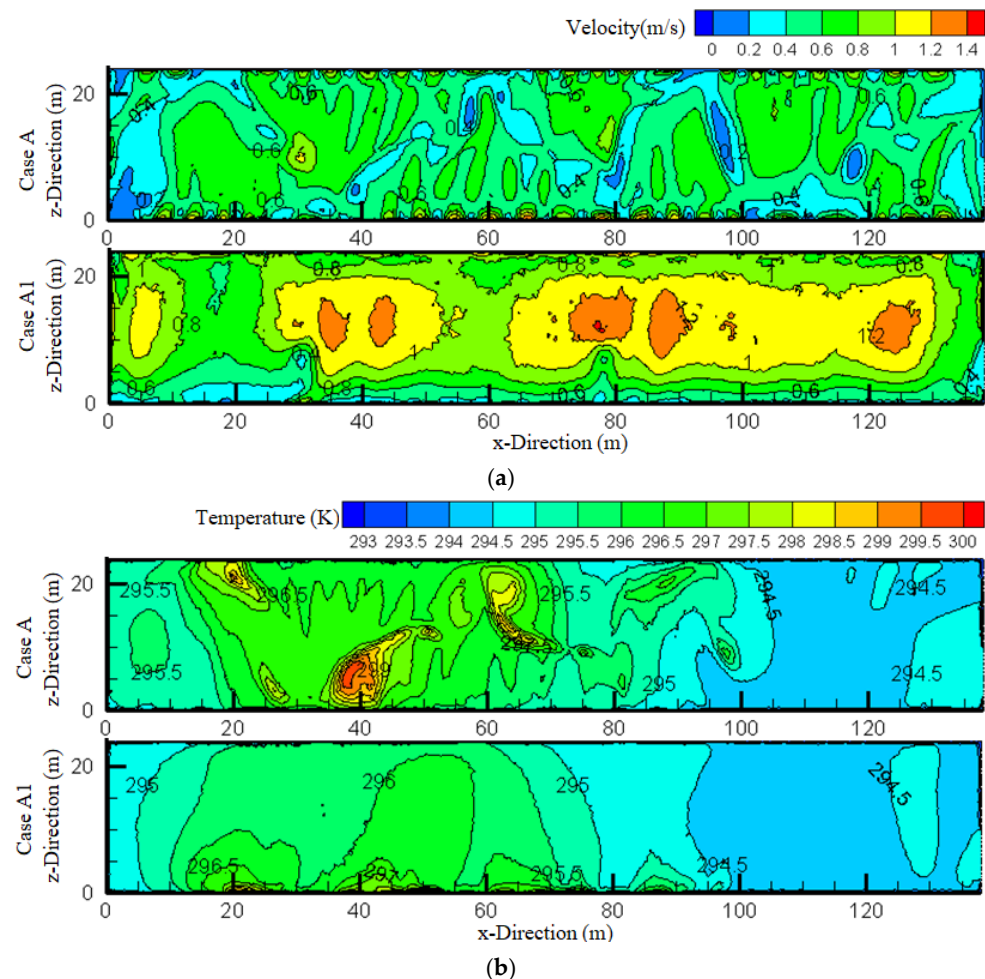


Figure 21. Comparison of air supply modes between double-sided (Case A) and single-sided (Case A1): (a) cloud diagram of velocity distribution; and (b) cloud diagram of temperature distribution.

Table 5 summarizes the assessment metrics for the two air supply modes under different opening configurations. The head-foot temperature difference and PD remained within the required design standards. Notably, η is higher in the single-sided mode

(Case A1, D1, E1, and F) compared to the double-sided mode (Case A, D, and E). For the single-sided mode, with the increase in the opening outlets, the energy utilization coefficient first increases and then decreases. In the scenario where the air supply outlets are opened at intervals of two (Case D1), η and APDI reach maximum values of 4.84 and 72.5%, respectively. An increased number of air supply openings enhanced heat exchange in the working area, resulting in improved air distribution uniformity, especially when all air supply outlets were fully open. The maximum increment in η was 43% (Case D1), the maximum reduction in Kv was 47% (Case D1), and the maximum reduction in Kt was 21% (Case D1). Overall, the uniformity of the single-sided mode surpasses that of the double-sided mode.

Table 5. Evaluation indicators under different opening modes.

Case	Head-Foot Temperature Difference (Δt)	Percentage of Dissatisfaction (%)	Energy Utilization Coefficient (η)	Velocity Non-Uniformity Coefficient (Kv)	Temperature Non-Uniformity Coefficient (Kt)	Air Diffusion Performance Index (ADPI) (%)	Percentage of Dissatisfaction (%)	Air Diffusion Performance Index (ADPI) (%)
A	0.55	0.5020	1.02	0.2583	0.0035	62.5	0.5020	62.5
D	0.42	0.4494	0.92	0.4216	0.0044	45	0.4494	45
E	0.33	0.4162	1.05	0.4390	0.0055	50	0.4162	50
A1	0.57	0.5106	3.38	0.2090	0.0024	70	0.5106	70
D1	0.71	0.5753	4.84	0.2686	0.0029	72.5	0.5753	72.5
E1	0.65	0.5166	3.26	0.3957	0.0035	55	0.5166	55
F	1.22	0.8874	3.54	0.3997	0.0036	42.5	0.8874	42.5

5. Conclusions

In this paper, the air distribution characteristics in the tall space of the underground generator layer under vertical wall-attached air supply were studied. By comparing the effects of the air supply velocity, outlet position, and opening mode, the layout of the vertical wall-attached air supply mode in a tall space was optimized. The conclusions are as follows:

- (1) In the single-sided vertical wall-attached ventilation mode, the head-foot temperature difference and PD could all meet the requirements of the relevant specifications. When the velocity was increased from 4 m/s to 8 m/s, the maximum increment in η was 41%, the maximum reduction in Kv was 9.5%, the maximum reduction in Kt was 34%, and the ADPI value reached 70%. With an increase in the number of outlet openings, the maximum increment of η was 43%, the maximum reduction in Kv was 47%, the maximum reduction in Kt was 21%, and the ADPI reached its maximum value of 72.5%.
- (2) In the double-sided vertical wall-attached air supply mode, the head-foot temperature difference and PD and ADPI value became smaller than that in the single-sided mode, changing the air supply velocity and air supply opening has little effect on η , and the variation trend of Kv and Kt was consistent with the single-sided mode.
- (3) Compared with the double-sided vertical wall-attached air supply, the single-sided mode energy utilization coefficient was higher, which could make the heat exchange in the generator layer working area more efficient. The working area's mean airflow velocity was higher than in the double-sided mode. However, when the number of outlet openings changed, the overall temperature change in the working area was not obvious in the single-sided mode.

To sum up, considering the mean temperature, mean airflow velocity, and evaluation indicators in the working zone, it is suggested to adopt the single-sided mode for this kind of tall space building, with an air supply velocity of $v = 6$ m/s and two open air supply outlets at each interval. The conclusions and suggestions in this paper are mainly applicable to the optimization of ventilation system of deep underground buildings, especially for underground hydropower stations.

Finally, the authors are definitely aware that the above-mentioned conclusions with detailed parameters refer to the specific conditions under research. But, the summary

of related overall variations may be pertinent for existing practical applications of ventilation modes. In the future, more research in this field needs to be examined with regard to the inlet air temperature, attached angle, and so on, to make the conclusions more comprehensive.

Author Contributions: Data curation, M.L.; formal analysis, M.L.; funding acquisition, T.R. and P.S.; methodology, T.R. and P.S.; software, M.L. and L.H.; validation, M.L.; writing—original draft, T.R. All authors have read and agreed to the published version of the manuscript.

Funding: This research was funded by the Natural Science Basic Research Program of Shaanxi Province (No.2022JQ-465) and the Natural Science Basic Research Program of Shaanxi Province (No.2022JQ-539).

Data Availability Statement: The data that support the findings of this study are available from the corresponding author, upon reasonable request.

Conflicts of Interest: The authors declare no conflict of interest.

References

- China Building Energy Efficiency Association Building Energy Consumption and Carbon Emission Data Special Committee. *Research Report of China Building Energy Consumption and Carbon Emissions*; China Building Energy Efficiency Association Building Energy Consumption and Carbon Emission Data Special Committee: Chongqing, China, 2022.
- Asim, N.; Badiei, M.; Mohammad, M.; Razali, H.; Rajabi, A.; Haw, L.C.; Ghazali, M.J. Sustainability of heating, ventilation and air-conditioning (HVAC) systems in buildings—An overview. *Int. J. Environ. Res. Public Health* **2020**, *19*, 1016. [[CrossRef](#)] [[PubMed](#)]
- Dong, J.K.; Gao, Y.; Sun, D.N.; Jiang, Y.Q.; Huang, S. Overview of implications, targets and technical paths of carbon neutrality in building sector. *Heat. Vent. Air Cond. (HVAC)* **2023**, *10*, 69–78.
- Xu, G.Y. Problems in HVAC design under concept of carbon neutrality. *Energy Energy Conserv.* **2022**, *12*, 29–131+135.
- Wang, Y.; Mauree, D.; Sun, Q.; Lin, H.; Scartezzini, J.L.; Wennersten, R. A review of approves to low carbon transition of high-rise residual builds in China. *Renew. Sustain. Energy Rev.* **2020**, *131*, 109990. [[CrossRef](#)]
- Ahn, H.; Rim, D.; Lo, L.J. Ventilation and energy performance of partitioned indoor spaces under mixing and displacement ventilation. *Build Simul.* **2018**, *11*, 561–574. [[CrossRef](#)]
- Cho, H.; Cabrera, D.; Sardy, S.; Kilchherr, R.; Yilmaz, S.; Martin, K.P. Evaluation of performance of energy efficient hybrid ventilation system and analysis of failants' behavior to control windows. *Build. Environ.* **2021**, *188*, 107434. [[CrossRef](#)]
- Zha, X.S.; Chen, Y.; Xie, F.X. Design and optimization of ventilation system for dam gallery of a hydropower station. *Refriger. Air Cond.* **2023**, *1*, 64–67.
- He, Q.Y.; Li, B.; Ang, J. Research on intelligent ventilation control of underground building of hydropower station based on deep learning. *Heat. Vent. Air Cond. (HVAC)* **2023**, *53* (Suppl. S1), 254–257.
- Wang, J. Study on Intelligent Control of Ventilation System for Underground Powerhouse of Hydropower Station. Master's Thesis, Huazhong University of Science & Technology, Wuhan, China, 2021.
- Liu, Y.N.; Xiao, Y.M.; Chen, J.L.; Augenbroe, G.; Zhou, T.C. A network model for natural ventilation simulation in deep buried underground structures. *Build. Environ.* **2019**, *153*, 288–301. [[CrossRef](#)]
- Wu, H.; Liu, J.; Wang, X.G.; Liu, L.H.; Tian, Z.H. In Situ Monitoring and Numerical Experiments on Vertical Deformation Profiles of Large-Scale Underground Caverns in Giant Hydropower Stations. *Geofluids* **2021**, *2021*, 6673825. [[CrossRef](#)]
- Xia, Y.M.; Xiao, X.M.; Zhang, Y.Z.; Wang, S.Y.; Lin, L.K. Numerical Simulation of Ventilation Performance for Large-scale Underground Cavern Group Considering Effect of Ventilation Shaft Structure. *Arab. J. Sci. Eng.* **2022**, *47*, 4093–4104. [[CrossRef](#)]
- Wang, Z.F.; Liu, Y.; Lei, T.; Gong, S.Q.; Ding, Y.; Wang, J.M.; Mo, W.J.; Xing, J.L. Study on ventilation and air conditioning strategy model test in underground hydropower station under part generator operation condition. *Heat. Vent. Air Cond. (HVAC)* **2018**, *4*, 71–75+124.
- Fu, X.Z.; Ding, Y.R. Discussion on air quality and thermal and humidity environment control design of residential buildings in hot summer and cold winter zone. *Heat. Vent. Air Cond. (HVAC)* **2021**, *10*, 58–63.
- Cheng, Z.; Li, L.L.; Qi, X.L.; Zhang, P.F. Research on the influence of ventilation opening shape on the wind pressure ventilation effect of gymnasium. *Build. Sci.* **2020**, *36*, 106–111+146. [[CrossRef](#)]
- Wang, H.D.; Hu, H.; Zhu, J.K.; Yang, X.Q.; Wang, R.K. Study on inter-zonal heat transfer for large space buildings with floor-level side wall air-supply system. *J. Refriger.* **2022**, *2*, 89–96.
- Huang, C.; Fan, Q.H.; Li, J.L.; Yue, J.; Wang, F.; Zou, Z.J.; Zhu, J.Y.; Miao, Y.F. B-G model of total heat in winter for large space buildings with low-side wall air supply systems. *Heat. Vent. Air Cond. (HVAC)* **2022**, *10*, 135–143.
- Sun, Y.X.; Yin, H.G.; Chen, T.; Wu, R.; Li, A.G. Ventilation effectiveness and human thermal comfort of displacement ventilation mode based on square column attachment. *Heat. Vent. Air Cond. (HVAC)* **2018**, *7*, 105–110.

20. Dong, Z.W.; Zhang, L.T.; Yang, Y.W.; Li, Q.F.; Huang, H. Numerical study on coupled operation of stratified air distribution system and natural ventilation under multi-variable factors in large space buildings. *Energies* **2021**, *14*, 8130. [[CrossRef](#)]
21. Ye, X.; Qi, H.C.; Kang, Y.M.; Zhong, K. Optimization study of heating performance for an impinging jet ventilation system based on data-driven model coupled with TOPSIS method. *Build. Environ.* **2022**, *22*, 109465. [[CrossRef](#)]
22. Yamasawa, H.; Kobayashi, T.; Yamanaka, T.; Choi, N.; Cehlin, M.; Ameen, A. Prediction of thermal and contaminant environment in a room with impinging jet ventilation system by zonal model. *Build. Environ.* **2022**, *221*, 109298. [[CrossRef](#)]
23. Thysen, J.-H.; Hooff, T.V.; Blocken, B.; Heijst, G.V. PIV measurements of opposing-jet ventilation flow in a reduced-scale simplified empty airplane cabin. *Eur. J. Mech. B/Fluids* **2022**, *94*, 212–227. [[CrossRef](#)]
24. Ameen, G.V.; Cehlin, M.; Larsson, U.; Yamasawa, H.; Kobayashi, T. Numerical investigation of the flow behavior of an isothermal corner impinging jet for building ventilation. *Build. Environ.* **2022**, *223*, 109486. [[CrossRef](#)]
25. Gu, J.Y.; Xie, D.Y.; Wang, L.Y.; Fan, J.W. CFD numerical simulation of ship engine room with jet ventilation system. *Ship Sci. Technol.* **2023**, *45*, 46–50.
26. Andersson, H.; Kabanshi, A.; Cehlin, M.; Moshfegh, B. On the ventilation performance of low momentum confluent jets supply device in a classroom. *Energies* **2020**, *13*, 5415. [[CrossRef](#)]
27. Wang, X.D.; Li, H.; Dong, J.L.; Wu, J.Q.; Tu, J.Y. Numerical study on mixing flow behavior in gas-liquid ejector. *Exp. Comput. Multiph. Flow* **2021**, *3*, 108–112. [[CrossRef](#)]
28. Tan, D.Y.; Li, B.Z.; Cheng, Y.; Liu, H.; Chen, J.H. Airflow pattern and performance of wall confluent jets ventilation for heating in a typical office space. *Indoor Built Environ.* **2019**, *29*, 67–83. [[CrossRef](#)]
29. Yin, H.G.; Wu, R.; Li, L.N.; Wang, Y.Y.; Li, A.G. Study on air flow structure characteristics of cylindrical attached ventilation under different column layout modes. *Heat. Vent. Air Cond. (HVAC)* **2020**, *50*, 120–124+132.
30. Yin, H.G.; Li, L.N.; Wu, R.; Wang, Y.Y.; Li, A.G. A numerical study on the effect of column layout on air distribution and performance of column attachment ventilation. *Build. Simul.* **2021**, *14*, 1095–1108. [[CrossRef](#)]
31. Han, O.; Li, A.G.; Yin, H.G. Comparative studies on isothermal attachment ventilation based on vertical walls, square and circular columns. *Energy Build.* **2021**, *231*, 110634.
32. Karimipannah, T.; Awbi, H.B. Theoretical and experiential investigation of impinging jet ventilation and comparison with wall placement ventilation. *Build. Environ.* **2022**, *37*, 1329–1342. [[CrossRef](#)]
33. He, X.J. Comparison of Airflow Organization Performance of Vertical Wall Attached Ventilation, Displacement Ventilation and Mixed Ventilation. Master's Thesis, Xi'an University of Architecture and Technology, Xi'an, China, 2020.
34. Ye, M.; Chen, T.; Zhong, K. Numerical study of thermal environment characteristics with impinging jet ventilation system in office buildings. *Vent. Air Cond.* **2021**, *40*, 30–34.
35. Han, T.; Deng, H.N.; Li, A.G.; Liu, H.; Du, H. Measurement and comparison of thermal environment and ventilation performance under different heating air supply modes of wall attached ventilation and mixed ventilation. *Heat. Vent. Air Cond. (HVAC)* **2021**, *10*, 138–144.
36. Han, T.; Xiong, J.G.; Deng, H.N.; Li, A.G. CFD simulation of horizontal attachment distance and thermal environment characteristics of rooms with vertical wall attached ventilation in heating mode. *Heat. Vent. Air Cond. (HVAC)* **2021**, *8*, 130–136+113.
37. Cao, G.Y.; Ruponen, M.; Kurnitski, J. Experiential investigation of the velocity distribution of the attached plane jet after impingement with the corner in a high room. *Energy Build.* **2010**, *42*, 935–944. [[CrossRef](#)]
38. Yin, H.G.; Chen, T.; Sun, Y.X.; Li, A.G. Analysis on air distribution characteristics of vertical wall attached air supply pattern and its influence factors. *Build. Sci.* **2016**, *8*, 33–39.
39. Li, A.G.; Ren, T.; Yang, C.Q.; Xiong, J.; Tao, P. Numerical simulation, PIV measurements and analysis of air movement influenced by nozzle jets and heat sources in underground generator hall. *Build. Environ.* **2018**, *131*, 16–31. [[CrossRef](#)]
40. Yin, H.G.; Li, A.G. Study of attached air curtain ventilation within a full-scale enclosure: Comparison of four turbulence models. *Indoor Built Environ.* **2016**, *25*, 962–975. [[CrossRef](#)]
41. Ren, T. Study on the Variation Characteristic and Distribution Law of Thermal and Humidity Environment for Underground Corridor/Cavern Based on Hydropower Engineering. Doctoral Thesis, Xi'an University of Architecture and Technology, Xi'an, China, 2016.
42. Wu, Y.; Gao, N.P.; Niu, J.L.; Zang, J.B.; Cao, Q. Numerical study on natural ventilation of the wind tower: Effects of combining with different window configurations in a low-rise house. *Build. Environ.* **2021**, *188*, 107450. [[CrossRef](#)]
43. Zhang, C.; Li, A.G.; Li, J.X.; Li, H.M.; Li, Y.; Xiong, J.; Lv, W.C.; Che, J.G.; Guo, J.N.; Zhang, X.Y. Optimization and analysis of the acoustic and resistance performance of the plenum chamber via sample entropy and large eddy simulation. *Build. Environ.* **2022**, *207*, 108545. [[CrossRef](#)]
44. Guo, J.N.; Li, A.G.; Ma, Y.Q.; Che, J.G.; Li, J.X.; Niu, S.F.; Deng, L.H.; Wang, D.; Che, L.F. A theoretical and applied convective heat transfer model for deep-buried underground tunnels with non-constant wall temperature. *Energy Build.* **2023**, *294*, 113210. [[CrossRef](#)]
45. Li, Y.J. Study on Cooling Characteristics of Non-Isothermal Wall-Mounted Attached Night Ventilation. Master's Thesis, Southwest Jiaotong University, Chengdu, China, 2021.
46. Gao, P. Research on Air Distribution of Hot Air Jet Units in Tall Factory Building. Master's Thesis, Xi'an University of Architecture and Technology, Xi'an, China, 2020.

47. Li, A.G.; Yang, C.Q.; Ren, T. Modeling and parametric studies for convective heat transfer in large, long and rough circular cross-sectional underground tunnels. *Energy Build.* **2016**, *127*, 259–267. [[CrossRef](#)]
48. Wang, J.L.; Yin, H.G.; Huo, Y.K.; Zhang, J.Y.; Liang, L.F.; Ji, D.N.; Chang, Z.; Ma, Z.J.; Li, A.G. Numerical investigation on air distribution characteristics and effect of the outlet opening mode on cross-shaped column attachment ventilation. *Build. Environ.* **2023**, *233*, 110086. [[CrossRef](#)]

Disclaimer/Publisher’s Note: The statements, opinions and data contained in all publications are solely those of the individual author(s) and contributor(s) and not of MDPI and/or the editor(s). MDPI and/or the editor(s) disclaim responsibility for any injury to people or property resulting from any ideas, methods, instructions or products referred to in the content.